

# AI-enhanced Direct SLAM: A Principled Approach to Unsupervised Learning in Bayesian Inference

Alexander Venus\*, Benjamin Deutschmann\*, Alexander Fuchs<sup>+</sup>, Christian Knoll<sup>+</sup>, and Erik Leitinger\*

\*Institute of Comm. Networks and Satellite Comms., Graz University of Technology, Austria, <sup>+</sup>Levata GmbH

Email: {a.venus,benjamin.deutschmann,erik.leitinger}@tugraz.at, {fuchs,knoll}@levata.at

**Abstract**—In this paper, we propose an artificial intelligence (AI)-enhanced hybrid simultaneous localization and mapping (SLAM) method that performs Bayesian inference directly on raw radio-frequency (RF) signals while learning an environment model in an unsupervised manner. The approach combines a physically interpretable signal model for line-of-sight (LOS) components with an AI model that captures multipath component statistics. Building on this formulation, we develop a particle-based sum-product algorithm (SPA) on a factor graph that jointly estimates the mobile terminal (MT) state, visibility, multipath parameters, and noise variances, and integrate it into a variational framework that maximizes the evidence lower bound (ELBO) to learn the neural network (NN) parametrization directly from measurements. We further present a highly efficient GPU-based implementation that enables parallel likelihood evaluation across particles and base stations (BSs). Simulation results in multipath environments demonstrate that the proposed method learns the generative, environment-dependent signal model in an unsupervised manner while accurately localizing the MT and effectively exploiting the learned map in obstructed-line-of-sight (OLOS) scenarios.

## I. INTRODUCTION

Accurate localization of mobile terminals (MTs) and situational awareness of the surrounding propagation environment are key enablers for future 6G communication networks, supporting applications such as autonomous navigation, indoor localization, digital twinning, and integrated sensing and communications [1]. While conventional positioning techniques perform well in open environments, their reliability degrades in urban and industrial scenarios as well as indoor environments due to multipath propagation and obstructed-line-of-sight conditions. Yet, multipath propagation also carries rich geometric information that can be exploited for localization [2], [3].

Multipath-based simultaneous localization and mapping (MP-SLAM) exploits reflected multipath components (MPCs) from map features such as virtual anchors (VAs), point scatterers, or simple surface models to jointly infer the MT state and environment from estimated MPC parameters (such as time-of-arrival (ToA), direction-of-arrival (DoA), direction-of-departure (DoD), or Doppler) [4], [5] within a Bayesian framework, and is often solved through belief propagation (BP) on a factor graph [6]–[8] or random finite sets (RFS) statistics [9], [10]. However, commonly used parametric models compress the true propagation environment into a few geometric features and thus fail to capture fine-grained electromagnetic effects such as diffuse multipath, material-dependent scattering, extended structures, as well as hardware imperfections. The same limitation persists in direct MP-SLAM [8]: although the likelihood is evaluated on raw RF signals, the underlying

generative model remains overly idealized, leading to model mismatch and calls for learnable environment representations.

Recent advances in AI demonstrate that purely data-driven models can enable RF signal-based localization [11], [12], yet they require large labeled data sets or often generalize poorly under domain shifts. This has motivated hybrid methods that retain physically interpretable models while learning only components that are difficult to model analytically [13]–[18]. For environment learning and mapping, a promising training objective is the marginal likelihood (evidence) of the received data under a latent-variable generative model. Since direct evidence maximization is intractable, variational inference maximizes an ELBO [19], enabling principled unsupervised learning via variational methods [20], [21]. Unlike supervised localization networks, ELBO-based learning “probabilistically matches” the learned generative model and the observed data.

In this work, we propose an *AI-enhanced SLAM* method that tightly couples Bayesian inference with unsupervised environment learning, eliminating the need for large sets of labeled MT positions and explicit geometric map information. Therefore, we consider a measurement likelihood function that combines model-based components (capturing the LOS contribution) with learned AI components (capturing the environment-induced MPCs). This allows us to retain a physically consistent signal model that explicitly models the sampled RF signal spectrum and array response and that learns the environment in terms of amplitude statistics and propagation geometry. The proper combination of both components is then enforced by a joint statistical model, expressed as type-II likelihood function [4], [5], [8], with its covariance matrix fusing model-based and learned contributions. We formulate the problem as a Bayesian inference task on a factor graph that directly takes the raw RF signals as input. Consequently, we can use particle-based SPA as an effective framework for joint optimization, i.e., analytical inference of the posterior PDF in combination with principled unsupervised learning of the AI components by maximization of the data evidence via the ELBO. Besides its conceptual elegance, this joint hybrid model on top of the proposed factor graph admits a computationally efficient GPU-based implementation with parallelization across particles and BSs. The main contributions are summarized as follows.

- We propose an AI-enhanced SLAM method that combines a physically interpretable signal model with NN models.
- We develop a factor graph-based particle SPA with computationally efficient covariance evaluation for scalable inference directly on raw RF measurements.
- We introduce an unsupervised learning approach that maximizes the ELBO to learn the propagation geometry and amplitude statistics directly from RF signals.
- We present an efficient GPU-based implementation enabling parallel likelihood evaluation across particles and BSs.

The project has received funding in part from the Austrian Research Promotion Agency (FFG) under the PRISM project (620753) and in part by the European Union’s Horizon Europe research and innovation program under Grant 101192113.

## II. SYSTEM MODEL AND PROBLEM FORMULATION

Each BS  $j$  located at known position  $\mathbf{p}^{(j)} \in \mathbb{R}^d$  transmits a signal with center frequency  $f_c$  and bandwidth  $B$ , which is received by a single MT at unknown position  $\mathbf{p}_k \in \mathbb{R}^d$ . In frequency domain, the transmitted baseband signal is denoted by  $S(f) \in \mathbb{C}$ . At each time step  $k$ ,  $M$  samples of the received signal waveform are recorded at the MT. This results in  $M_f = B/\Delta + 1$  samples with frequency spacing  $\Delta$  (the unambiguous observation distance is given by  $d_{\max} = c/\Delta$ , where  $c$  is the speed of light). The MT is equipped with an antenna array comprising  $M_a$  elements, located at positions  $\mathbf{a}_m \in \mathbb{R}^d$  with  $m \in \{1, \dots, M_a\}$  (within the frame of reference of the MT). The array center is defined to be  $\frac{1}{M_a} \sum_{m=1}^{M_a} \mathbf{a}_m = \mathbf{0}$ . In the global coordinate system at time  $k$ , the array orientation is denoted by  $o_k$  and the array center is at  $\mathbf{p}_k$ .

The RF signal model for the sampled received signal with respect to BS  $j$ , i.e.,  $\mathbf{z}_k^{(j)} = [z_k^{(j)}(-M-1)/2\Delta \cdots z_k^{(j)}((M-1)/2\Delta)]^T = [z_{k,1}^{(j)} \cdots z_{k,M}^{(j)}]^T$  comprising the LOS component and a superposition of  $L_k^{(j)} - 1$  MPCs can be expressed as [8]

$$\mathbf{z}_k^{(j)} = \sum_{l=1}^{L_k^{(j)}} \varrho_{l,k}^{(j)} \mathbf{h}_{\mathcal{X}}(\tau_{l,k}^{(j)}, \mathbf{u}_{l,k}^{(j)}) + \boldsymbol{\epsilon}_k^{(j)} \quad (1)$$

where  $\tau_{l,k}^{(j)}$  is the delay,  $\mathbf{u}_{l,k}^{(j)}$  is the DoA, and  $\varrho_{l,k}^{(j)} \in \mathbb{C}$  is the complex amplitude of the  $l$ -th MPC and  $\boldsymbol{\epsilon}_k^{(j)} \sim \mathcal{CN}(\mathbf{0}, \eta_k^{(j)} \mathbf{I})$  is additive noise. Assuming a planar-wave, narrow-band signal model [22], the according joint frequency–array response vector  $\mathbf{h}_{\mathcal{X}}(\tau, \mathbf{u})$  with length  $M = M_f M_a$  related to the parameter ToA  $\tau$  and DoA  $\mathbf{u}$  of an MPC factorizes as

$$\mathbf{h}_{\mathcal{X}}(\tau, \mathbf{u}) = \mathbf{h}_{\mathcal{X}_f}(\tau) \otimes \mathbf{a}_{\mathcal{X}_u}(\mathbf{u}) \in \mathbb{C}^M \quad (2)$$

where the vector  $\boldsymbol{\chi} = [\boldsymbol{\chi}_f^T \cdots \boldsymbol{\chi}_u^T]^T$  contains unknown parameters of the response vector and  $\mathbf{h}_{\mathcal{X}_f}(t) \in \mathbb{C}_f^M$  denotes the sampled transmitted signal delayed by the ToA  $\tau$ , i.e.,

$$\mathbf{h}_{\mathcal{X}_f}(\tau) = \frac{c}{4\pi f_c \tau} [w_{f,1} S(- (M_f - 1)/2\Delta) e^{j2\pi(M_f-1)/(2\Delta)\tau} \cdots w_{f,M_f} S((M_f - 1)/2\Delta) e^{-j2\pi(M_f-1)/(2\Delta)\tau}]^T \quad (3)$$

where  $c/(4\pi f_c \tau)$  accounts for the path-loss and  $\boldsymbol{\chi}_f = [w_{f,1} \cdots w_{f,M_f}]^T$ . The proposed method can also be extended to unsynchronized systems [3], [9], [23]. The array response  $\mathbf{a}_{\mathcal{X}_u}^{(j)}(\mathbf{u})$  for direction  $\mathbf{u} \in \mathbb{R}^d$  with  $\|\mathbf{u}\| = 1$  is given by

$$\mathbf{a}_{\mathcal{X}_u}(\mathbf{u}) = [w_{u,1} e^{-j\frac{2\pi}{\gamma_c} \mathbf{u}^T (\mathbf{a}_1 + \Delta \mathbf{a}_1)} \cdots w_{u,M_a} e^{-j\frac{2\pi}{\gamma_c} \mathbf{u}^T (\mathbf{a}_{M_a} + \Delta \mathbf{a}_{M_a})}]^T \quad (4)$$

where  $\boldsymbol{\chi}_u = [w_{u,1} \cdots w_{u,M_a} \Delta \mathbf{a}_1^T \cdots \Delta \mathbf{a}_{M_a}^T]^T$ . The geometry dimension  $d$  is specified by the specific scenario (2D or 3D).

### A. AI-augmented Measurement Model and State Vectors

By separating the LOS component from the MPC component and explicitly combining the frequency–array response vector in (2) with AI-based models for the MPC contribution, the signal model in (1), conditioned on the MT position  $\mathbf{p}_k$  and orientation  $o_k$ , can be rewritten as<sup>1</sup>

$$\mathbf{z}_k^{(j)} = r_k^{(j)} \rho_{\text{los},k}^{(j)} \mathbf{h}_{\mathcal{X}}^{\text{lo}(j)}(\mathbf{p}_k) + \sum_{n=1}^D \rho_{\boldsymbol{\theta},n}^{\text{ai}(j)} \mathbf{h}_{\boldsymbol{\theta},n}^{\text{ai}(j)}(\mathbf{p}_k) + \boldsymbol{\epsilon}_k^{(j)} \quad (5)$$

where  $\mathbf{h}_{\mathcal{X}}^{\text{lo}(j)}(\mathbf{p}_k) \triangleq \mathbf{h}_{\mathcal{X}}(\tau_{\text{lo},k}^{(j)}, \mathbf{u}_{\text{lo},k}^{(j)}) \in \mathbb{C}^M$  denotes the signal contribution from the LOS of BS  $j$ . This term is

parameterized by the delay  $\tau_{\text{lo},k}^{(j)} = \|\mathbf{p}^{(j)} - \mathbf{p}_k\|/c$  and the DoA  $\mathbf{u}_{\text{lo},k}^{(j)} = \mathbf{R}(o_k)(\mathbf{p}^{(j)} - \mathbf{p}_k)/\|\mathbf{p}^{(j)} - \mathbf{p}_k\|$ , where the rotation matrix  $\mathbf{R}(o_k)$  transforms the direction from the MT local coordinate system to the global coordinate system according to the MT orientation  $o_k$ . The response vector accounting for neural-enhanced (NE) components is given by  $\mathbf{h}_{\boldsymbol{\theta},n}^{\text{ai}(j)}(\mathbf{p}_k) \triangleq \mathbf{h}_{\mathcal{X}}(\tau_{\boldsymbol{\theta},n,k}^{\text{ai}(j)}, \mathbf{u}_{\boldsymbol{\theta},n,k}^{\text{ai}(j)}) \in \mathbb{C}^M$  with  $\tilde{\boldsymbol{\theta}} = [\boldsymbol{\chi}^T \boldsymbol{\theta}^T]^T$  denotes the contribution vector related to MPC originating from the surrounding propagation environment with parameters  $\tau_{\boldsymbol{\theta},n,k}^{\text{ai}(j)} = \|\mathbf{p}_{\boldsymbol{\theta},n}^{\text{ai}(j)} - \mathbf{p}_k\|/c + b_{\boldsymbol{\theta},n}^{\text{ai}(j)}$  and  $\mathbf{u}_{\boldsymbol{\theta},n,k}^{\text{ai}(j)} = \mathbf{R}(o_k)(\mathbf{p}_{\boldsymbol{\theta},n}^{\text{ai}(j)} - \mathbf{p}_k)/\|\mathbf{p}_{\boldsymbol{\theta},n}^{\text{ai}(j)} - \mathbf{p}_k\|$  with neural map feature positions  $\mathbf{p}_{\boldsymbol{\theta},n}^{\text{ai}(j)} \in \mathbb{R}^{d \times 1}$  and biases  $b_{\boldsymbol{\theta},n}^{\text{ai}(j)} \in \mathbb{R}$  describing the geometry of the propagation environment represented by data-driven machine learning (ML) model given by

$$\mathbf{P}_{\boldsymbol{\theta}}^{\text{ai}(j)} = \mathbf{f}_{\mathbf{p},\boldsymbol{\theta}}^{\text{ai}(j)}(\mathbf{p}^{(j)}) \in \mathbb{R}^{d+1 \times D} \quad (6)$$

where  $\mathbf{P}_{\boldsymbol{\theta}}^{\text{ai}(j)} = [[\mathbf{p}_{\boldsymbol{\theta},1}^{\text{ai}(j)T} b_{\boldsymbol{\theta},1}^{\text{ai}(j)}] \cdots [\mathbf{p}_{\boldsymbol{\theta},D}^{\text{ai}(j)T} b_{\boldsymbol{\theta},D}^{\text{ai}(j)}]]^T$ . Note that (6) does not depend on the MT position, since it represents a MT position invariant map. The number of components  $D$  of the AI model is a design parameter discussed later in Section VI. The existence of the LOS component of each BS  $j$  is modeled by a binary random variable  $r_k^{(j)} \in \{0, 1\}$ . Thus, the direct path between MT and BS  $j$  exists and contributes to the received signal, if and only if  $r_k^{(j)} = 1$ .

We assume that the complex amplitudes,  $\rho_{\text{los},k}^{(j)}$  and  $\rho_{\boldsymbol{\theta},n}^{\text{ai}(j)}$ , are random and unknown [8], [24], [25]. In particular, random amplitudes are modeled by zero-mean complex Gaussian random variables  $\rho_{\text{los},k}^{(j)} \sim \mathcal{CN}(\rho_{\text{los},k}^{(j)}; 0, \gamma_k^{(j)})$  with amplitude variance  $\gamma_k^{(j)}$  and  $\rho_{\boldsymbol{\theta},n,k}^{\text{ai}(j)} \sim \mathcal{CN}(\rho_{\boldsymbol{\theta},n}^{\text{ai}(j)}; 0, \gamma_{\boldsymbol{\theta},n}^{\text{ai}(j)})$  with variance

$$\gamma_{\boldsymbol{\theta}}^{\text{ai}(j)} = \mathbf{f}_{\rho,\boldsymbol{\theta}}^{\text{ai}(j)}(\mathbf{p}^{(j)}) \in \mathbb{R}_+^{1 \times D} \quad (7)$$

represented by a data-driven ML model with  $\boldsymbol{\gamma}_{\boldsymbol{\theta}}^{\text{ai}(j)} = [\gamma_{\boldsymbol{\theta},1}^{\text{ai}(j)} \cdots \gamma_{\boldsymbol{\theta},D}^{\text{ai}(j)}]^T$ . Note that the amplitude model is assumed MT-position invariant due to pathloss compensation. To capture position-dependent variations caused by complex environment interactions and visibility changes of feature-related propagation paths, an additional position-dependent network can be incorporated. The amplitude model<sup>2</sup> is referred to as *Swerling 1* [26]. The complex amplitudes  $\rho_{\text{los},k}^{(j)}$  and  $\rho_{\boldsymbol{\theta},n}^{(j)}$  are independent across  $k, n$ , and  $j$ . The additive noise term  $\boldsymbol{\epsilon}_k^{(j)}$  is spatially white. Thus, it is distributed according to  $\mathcal{CN}(\boldsymbol{\epsilon}_k^{(j)}; \mathbf{0}, \eta_k^{(j)} \mathbf{I}_M)$  and independent across  $k$  and all  $j$ , as well as independent of all complex amplitudes with noise variance  $\eta_k^{(j)}$ .

From the signal model in (5), we obtain the probability density function (PDF) of the measurement  $\mathbf{z}_k^{(j)}$  conditioned on the MT state  $\mathbf{x}_k = [\mathbf{p}_k^T \mathbf{v}_k^T o_k]^T$  (containing respectively its position, velocity, and orientation), the LOS state  $\mathbf{y}_k^{(j)} = [r_k^{(j)} \gamma_k^{(j)}]^T$ , and the noise variance  $\eta_k^{(j)}$  to be zero-mean complex Gaussian PDF and given as

$$f_{\tilde{\boldsymbol{\theta}}}(\mathbf{z}_k^{(j)} | \mathbf{x}_k, \mathbf{y}_k^{(j)}, \eta_k^{(j)}) = \mathcal{CN}(\mathbf{z}_k^{(j)}; \mathbf{0}, \mathbf{C}_{\tilde{\boldsymbol{\theta}},k}^{(j)}(\mathbf{p}_k, \mathbf{y}_k^{(j)}, \eta_k^{(j)})) \quad (8)$$

<sup>2</sup>In the Swerling-1 model, the target reflectivity is modeled as a zero-mean circularly symmetric complex Gaussian random variable, which implies a uniformly distributed phase and a Rayleigh-distributed magnitude; by deliberately neglecting phase information and mean amplitude and characterizing the return solely through its variance (average power), the model is particularly robust against both amplitude and phase fluctuations.

<sup>1</sup>The proposed signal model can be straightforwardly extended to MIMO systems or adapted to include Doppler frequencies.

with covariance matrix

$$\mathbf{C}_{\hat{\theta},k}^{(j)}(\mathbf{p}_k, \mathbf{y}_k^{(j)}, \eta_k^{(j)}) = \eta_k^{(j)} \mathbf{I}_M + r_k^{(j)} \mathbf{C}_{\chi,k}^{(j)}(\mathbf{p}_k, \gamma_k^{(j)}) + \mathbf{C}_{\hat{\theta},k}^{\text{ai}(j)}(\mathbf{p}_k) \quad (9)$$

where

$$\mathbf{C}_{\chi,k}^{(j)}(\mathbf{p}_k, \gamma_k^{(j)}) = \gamma_k^{(j)} \mathbf{h}_{\chi}^{\text{lo}(j)}(\mathbf{p}_k) (\mathbf{h}_{\chi}^{\text{lo}(j)}(\mathbf{p}_k))^{\text{H}} \quad (10)$$

$$\mathbf{C}_{\hat{\theta},k}^{\text{ai}(j)}(\mathbf{p}_k) = \mathbf{P}_{\chi,k}^{(j)} \sum_{n=1}^D \gamma_{\hat{\theta},n}^{\text{ai}(j)} \mathbf{h}_{\hat{\theta},n}^{\text{ai}(j)}(\mathbf{p}_k) (\mathbf{h}_{\hat{\theta},n}^{\text{ai}(j)}(\mathbf{p}_k))^{\text{H}} \mathbf{P}_{\chi,k}^{(j)\text{H}} \quad (11)$$

with  $\mathbf{P}_{\chi,k}^{(j)} = \mathbf{I} - (\mathbf{h}_{\chi}^{\text{lo}(j)}(\mathbf{p}_k) \mathbf{h}_{\chi}^{\text{lo}(j)\text{H}}(\mathbf{p}_k)) / \|\mathbf{h}_{\chi}^{\text{lo}(j)}(\mathbf{p}_k)\|^2$  is the orthogonal projection operator that enforces that the data-driven covariance matrix is not reducing the position information of the LOS covariance matrix. Finally, we have  $f(\mathbf{z}_k | \mathbf{x}_k, \mathbf{y}_k) = \prod_{j=1}^J f(\mathbf{z}_k^{(j)} | \mathbf{x}_k, \mathbf{y}_k^{(j)}, \eta_k^{(j)})$ , where we introduced  $\mathbf{z}_k = [\mathbf{z}_k^{(1)\text{T}} \cdots \mathbf{z}_k^{(J)\text{T}}]^{\text{T}}$ ,  $\mathbf{y}_k = [\mathbf{y}_k^{(1)\text{T}} \cdots \mathbf{y}_k^{(J)\text{T}}]^{\text{T}}$ . Similarly, we also define  $\gamma_k = [\gamma_k^{(1)\text{T}} \cdots \gamma_k^{(J)\text{T}}]^{\text{T}}$ ,  $\mathbf{r}_k = [r_k^{(1)\text{T}} \cdots r_k^{(J)\text{T}}]^{\text{T}}$ , and  $\eta_k = [\eta_k^{(1)\text{T}} \cdots \eta_k^{(J)\text{T}}]^{\text{T}}$ .

The functional mappings  $f_{\mathbf{p},\theta}^{\text{ai}}(\mathbf{p}^{(j)})$  in (6) and  $f_{\rho,\theta}^{\text{ai}}(\mathbf{p}^{(j)})$  in (7) are implemented by deep NNs as described in Section VI. These models learn a position-dependent generative RF signal model that captures the propagation environment. In addition, the parameter vector  $\chi$  of the response vector in (2) can be optionally learned in a similar manner (cf. Section VI).

### B. State-Transition Models and Prior PDFs

The dynamics of the MT state  $\mathbf{x}_k = [\mathbf{p}_k^{\text{T}} \mathbf{v}_k^{\text{T}} o_k]^{\text{T}}$  are described by a first-order Markov model with state-transition PDF  $f(\mathbf{x}_k | \mathbf{x}_{k-1}, \mathbf{z}_o)$ , where  $\mathbf{z}_o$  is an inertial measurement unit (IMU)-based orientation measurement [27]. Each LOS state  $\mathbf{y}_k^{(j)}$ ,  $j \in \{1, \dots, J\}$ , and the noise variance are also assumed to evolve independently according to first-order Markov models with transition densities  $f(\eta_k^{(j)} | \eta_{k-1}^{(j)})$  and  $f(\gamma_k^{(j)} | \gamma_{k-1}^{(j)}) = f(\gamma_k^{(j)}, r_k^{(j)} | \gamma_{k-1}^{(j)}, r_{k-1}^{(j)})$ . If BS  $j$  is obstructed at time  $k-1$ , i.e.,  $r_{k-1}^{(j)} = 0$ , it becomes visible at time  $k$  with appearance probability  $0 < p_a \leq 1$  or remains obstructed with probability  $1 - p_a$ . The corresponding state-transition PDF for  $r_{k-1}^{(j)} = 0$  is thus given by

$$f(\gamma_k^{(j)}, r_k^{(j)} | \gamma_{k-1}^{(j)}, 0) = \begin{cases} (1 - p_a) f_{\text{D}}(\gamma_k^{(j)}), & r_k^{(j)} = 0 \\ p_a f_a(\gamma_k^{(j)}), & r_k^{(j)} = 1 \end{cases} \quad (12)$$

where  $f_{\text{D}}(\gamma_k^{(j)})$  is an arbitrary ‘‘dummy’’ PDF and  $f_a(\gamma_k^{(j)})$  is the PDF of  $\gamma_k^{(j)}$  if LOS of BS  $j$  appears (becomes visible). However, if the BS is visible at time step  $k-1$ , i.e.,  $r_{k-1}^{(j)} = 1$ , then it continues to be visible at time step  $k$  with visibility probability  $0 < p_v \leq 1$ . If it still exists at time  $k$ , then  $\gamma_k^{(j)}$  is distributed according to  $f(\gamma_k^{(j)} | \gamma_{k-1}^{(j)})$ . For  $r_{k-1}^{(j)} = 0$ , the state-transition PDF thus reads

$$f(\gamma_k^{(j)}, r_k^{(j)} | \gamma_{k-1}^{(j)}, 1) = \begin{cases} (1 - p_v) f_{\text{D}}(\gamma_k^{(j)}), & r_k^{(j)} = 0 \\ p_v f(\gamma_k^{(j)} | \gamma_{k-1}^{(j)}), & r_k^{(j)} = 1. \end{cases} \quad (13)$$

The temporal evolution of the LOS variance is described by a PDF  $f(\gamma_k^{(j)} | \gamma_{k-1}^{(j)}) = \mathcal{G}(\gamma_k^{(j)}; c_{\gamma}, \gamma_{k-1}^{(j)} / c_{\gamma})$  denoting a Gamma<sup>3</sup>

<sup>3</sup>The Gamma distribution is the conjugate prior for the variance of a complex Gaussian distribution.

PDF with mean  $\gamma_{k-1}^{(j)}$  and variance  $(\gamma_{k-1}^{(j)})^2 / c_{\gamma}$ . Similarly, the temporal dynamic of the noise variance is described by a PDF  $f(\eta_k^{(j)} | \eta_{k-1}^{(j)}) = \mathcal{G}(\eta_k^{(j)}; c_{\eta}, \eta_{k-1}^{(j)} / c_{\eta})$  with mean  $\eta_{k-1}^{(j)}$  and variance  $(\eta_{k-1}^{(j)})^2 / c_{\eta}$ . At time  $k = 0$ , the prior distributions  $f(\mathbf{x}_0)$ ,  $f(\eta_0^{(j)})$ ,  $j \in \{1, \dots, J\}$ , and  $f(\mathbf{y}_0^{(j)})$ ,  $j \in \{1, \dots, J\}$  are assumed known. The random variables  $\mathbf{x}_0$ ,  $\eta_0^{(j)}$ ,  $j \in \{1, \dots, J\}$ , and  $\mathbf{y}_0^{(j)}$ ,  $j \in \{1, \dots, J\}$  are all independent of each other.

### C. Declaration and Estimation

At each time step  $k$ , given all the measurements  $\mathbf{z}_{0:k} = [\mathbf{z}_1^{\text{T}} \cdots \mathbf{z}_k^{\text{T}}]^{\text{T}}$ , our goal is to estimate MT state  $\mathbf{x}_k$ , and the noise variance  $\eta_k^{(j)}$  and BS state  $\mathbf{y}_k^{(j)}$ . In our Bayesian setting, the problem comprises the computation of the marginal PDFs  $f(\mathbf{y}_k^{(j)} | \mathbf{z}_{1:k})$ ,  $f(\eta_k^{(j)} | \mathbf{z}_{1:k})$ , and  $f(\mathbf{x}_k | \mathbf{z}_{1:k})$  using all measurements  $\mathbf{z}_{1:k} \triangleq [\mathbf{z}_1^{\text{T}} \cdots \mathbf{z}_k^{\text{T}}]^{\text{T}}$ .

Based on these marginal PDFs, the minimum mean-square error (MMSE) estimate of the MT states, LOS states, and noise variances at time  $k$ , can be obtained as

$$\hat{\mathbf{x}}_{k,\text{MMSE}} = \int \mathbf{x}_k f(\mathbf{x}_k | \mathbf{z}_{1:k}) d\mathbf{x}_k \quad (14)$$

$$\gamma_{k,\text{MMSE}}^{(j)} = \int \gamma_k^{(j)} f(\gamma_k^{(j)} | r_k^{(j)} = 1, \mathbf{z}_{1:k}) d\gamma_k^{(j)} \quad (15)$$

$$\hat{\eta}_{k,\text{MMSE}}^{(j)} = \int \eta_k^{(j)} f(\eta_k^{(j)} | \mathbf{z}_{1:k}) d\eta_k^{(j)}. \quad (16)$$

The marginal PDF in (15) is obtained by  $f(\gamma_k^{(j)} | r_k^{(j)} = 1, \mathbf{z}_{1:k}) = f(\gamma_k^{(j)}, r_k^{(j)} = 1 | \mathbf{z}_{1:k}) / p(r_k^{(j)} = 1 | \mathbf{z}_{1:k})$ , where  $p(r_k^{(j)} | \mathbf{z}_{1:k}) = \int f(\gamma_k^{(j)}, r_k^{(j)} | \mathbf{z}_{1:k}) d\gamma_k^{(j)}$  is the marginal probability mass function (PMF) representing the BS visibility.

Following the statistical model and assumptions in Sections II-A to II-B, the joint posterior PDF  $f_{\hat{\theta}}(\mathbf{x}_{0:k}, \mathbf{y}_{0:k}, \boldsymbol{\eta}_{0:k} | \mathbf{z}_{1:k})$  with  $\mathbf{x}_{0:k} \triangleq [\mathbf{x}_0^{\text{T}} \cdots \mathbf{x}_k^{\text{T}}]^{\text{T}}$ ,  $\mathbf{y}_{0:k} \triangleq [\mathbf{y}_0^{\text{T}} \cdots \mathbf{y}_k^{\text{T}}]^{\text{T}}$ , and  $\boldsymbol{\eta}_{0:k} \triangleq [\eta_0^{\text{T}} \cdots \eta_k^{\text{T}}]^{\text{T}}$  can be factorized as

$$f_{\hat{\theta}}(\mathbf{x}_{0:k}, \mathbf{y}_{0:k}, \boldsymbol{\eta}_{0:k} | \mathbf{z}_{1:k}) = \frac{f_{\hat{\theta}}(\mathbf{x}_{0:k}, \mathbf{y}_{0:k}, \boldsymbol{\eta}_{0:k}, \mathbf{z}_{1:k})}{f_{\hat{\theta}}(\mathbf{z}_{1:k})} \times f(\mathbf{x}_0) \left( \prod_{j=1}^J f(\mathbf{y}_0^{(j)}) f(\eta_0^{(j)}) \right) \prod_{k'=1}^k f(\mathbf{x}_{k'} | \mathbf{x}_{k'-1}, \mathbf{z}_o) \times \prod_{j=1}^J f(\mathbf{y}_{k'}^{(j)} | \mathbf{y}_{k'-1}^{(j)}) f(\eta_{k'}^{(j)} | \eta_{k'-1}^{(j)}) f_{\hat{\theta}}(\mathbf{z}_{k'}^{(j)} | \mathbf{x}_{k'}, \mathbf{y}_{k'}^{(j)}, \eta_{k'}^{(j)}). \quad (18)$$

Two time steps of the factor graph corresponding to the factorization in (18), are shown in Fig. 1. This factorization facilitates the development of an efficient method for the computation of marginal posterior PDFs  $f(\mathbf{y}_k^{(j)} | \mathbf{z}_{1:k}) \approx \tilde{f}(\mathbf{y}_k^{(j)})$ ,  $f(\eta_k^{(j)} | \mathbf{z}_{1:k}) \approx \tilde{f}(\eta_k^{(j)})$ , and  $f(\mathbf{x}_k | \mathbf{z}_{1:k}) \approx \tilde{f}(\mathbf{x}_k)$ .

### III. SUM-PRODUCT ALGORITHM (SPA)

Since direct marginalization of the joint posterior PDF in (18) is infeasible, we use BP message passing by means of the SPA [28]–[30] and approximate the marginal posterior PDFs and messages, typically referred to as beliefs, by a particle-based representation. BP is an efficient approach for solving high-dimension Bayesian inference problems. A BP method is derived by performing local operations called ‘‘messages’’ on the edges of the factor graph [28]–[30] that represents

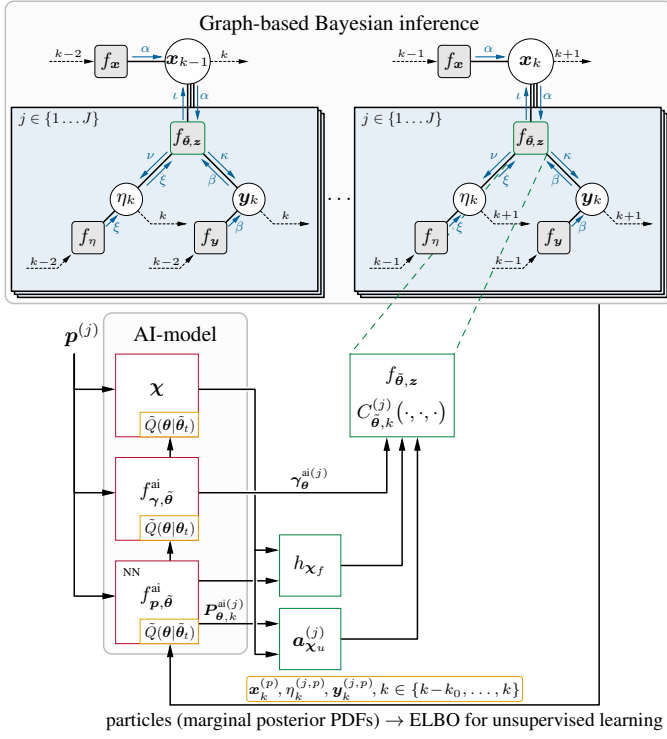


Fig. 1. Concept figure of two time steps of the proposed method, where NNs learn the environment to enhance the statistical measurement model. Top: factor graph and model-based components (measurement model in green) of the sum-product algorithm (SPA). Bottom: AI model in red (NNs and other learned parameters) and their links to the signal and likelihood model. Quantities associated with unsupervised learning are shown in orange.

the statistical model of the Bayesian estimation problem. We make use of the following message passing computation order: (i) messages are passed only forward in time, (ii) along the edges connecting an MT state variable node “ $\mathbf{x}_k$ ” and a BS-related variable node “ $\mathbf{y}_k^{(j)}$ ” or “ $\eta_k^{(j)}$ ” messages from other BS-related variable nodes “ $\mathbf{y}_k^{(j')}$ ” or “ $\eta_k^{(j')}$ ” with  $j' \neq j$  are not considered (c.f. [6]). BP messages are also shown in Fig. 1. They are computed in parallel for all BSs  $j \in \{1, \dots, J\}$ .

### A. Prediction Messages

First, we present the MT prediction message that is passed from factor node “ $f(\mathbf{x}_k | \mathbf{x}_{k-1})$ ” to variable node “ $\mathbf{x}_k$ ”. This message is obtained as

$$\alpha(\mathbf{x}_k) = \int f(\mathbf{x}_k | \mathbf{x}_{k-1}) \tilde{f}(\mathbf{x}_{k-1}) d\mathbf{x}_{k-1} \quad (19)$$

where  $\tilde{f}(\mathbf{x}_{k-1})$  is the belief of the MT state at the previous time step  $k-1$ . The prediction message of the BS states is

$$\beta(\mathbf{y}_k^{(j)}) = \sum_{r_{k-1}^{(j)} \in \{0,1\}} \int f(\gamma_k^{(j)}, r_k^{(j)} | \gamma_{k-1}^{(j)}, r_{k-1}^{(j)}) \times \tilde{f}(\gamma_{k-1}^{(j)}, r_{k-1}^{(j)}) d\gamma_{k-1}^{(j)} \quad (20)$$

where  $\tilde{f}(\mathbf{y}_{k-1}^{(j)}) = \tilde{f}(\gamma_{k-1}^{(j)}, r_{k-1}^{(j)})$  is the corresponding belief at time step  $k-1$ . Inserting (12) and (13) for  $f(\gamma_k^{(j)}, r_k^{(j)} | \gamma_{k-1}^{(j)}, 1)$  and  $f(\gamma_k^{(j)}, r_k^{(j)} | \gamma_{k-1}^{(j)}, 0)$ , we obtain for  $r_k^{(j)} = 1$

$$\beta(\gamma_k^{(j)}, 1) = p_v \int f(\gamma_k^{(j)} | \gamma_{k-1}^{(j)}) \tilde{f}(\gamma_{k-1}^{(j)}, 1) d\gamma_{k-1}^{(j)} + p_a \int f_a(\gamma_k^{(j)}) \tilde{f}(\gamma_{k-1}^{(j)}, 0) d\gamma_{k-1}^{(j)} \quad (21)$$

and, for  $r_k^{(j)} = 0$ , we have  $\alpha(\gamma_k^{(j)}, 0) = \alpha_k^{(j)} f_D(\gamma_k^{(j)})$  with

$$\beta_k^{(j)} = (1 - p_v) \int \tilde{f}(\gamma_{k-1}^{(j)}, 1) d\gamma_{k-1}^{(j)} + (1 - p_a) \int \tilde{f}(\gamma_{k-1}^{(j)}, 0) d\gamma_{k-1}^{(j)}. \quad (22)$$

Finally, for each  $j \in \{1, \dots, J\}$ , the prediction message that is sent from the factor node “ $f(\eta_k^{(j)} | \eta_{k-1}^{(j)})$ ” to the noise variance node “ $\eta_k^{(j)}$ ”, is given by

$$\xi(\eta_k^{(j)}) = \int f(\eta_k^{(j)} | \eta_{k-1}^{(j)}) \tilde{f}(\eta_{k-1}^{(j)}) d\eta_{k-1}^{(j)} \quad (23)$$

where  $\tilde{f}(\eta_{k-1}^{(j)})$  is the belief of the noise variance computed at the previous time step  $k-1$ .

### B. Measurement Update Messages

After prediction messages are obtained, a measurement update is performed where messages that provide the information of measurements  $\mathbf{z}_k$  are obtained. Specifically, messages sent from factor nodes “ $f(\mathbf{z}_k^{(j)} | \mathbf{x}_k, \mathbf{y}_k^{(j)})$ ” to MT state “ $\mathbf{x}_k$ ”, BS states “ $\mathbf{y}_k^{(j)}$ ,  $j \in \{1, \dots, J\}$ ” are computed. The messages  $\iota(\mathbf{x}_k; \mathbf{z}_k^{(j)})$ ,  $j \in \{1, \dots, J\}$  sent from “ $f(\mathbf{z}_k^{(j)} | \mathbf{x}_k, \mathbf{y}_k^{(j)}, \eta_k^{(j)})$ ” to “ $\mathbf{x}_k$ ” are obtained as

$$\iota(\mathbf{x}_k; \mathbf{z}_k^{(j)}) = \sum_{r_k^{(j)} \in \{0,1\}} \iint f(\mathbf{z}_k^{(j)} | \mathbf{x}_k, \gamma_k^{(j)}, r_k^{(j)}, \eta_k^{(j)}) \times \beta(\gamma_k^{(j)}, r_k^{(j)}) \xi(\eta_k^{(j)}) d\gamma_k^{(j)} d\eta_k^{(j)}. \quad (24)$$

Note that the measurements  $\mathbf{z}_k^{(j)}$ ,  $j \in \{1, \dots, J\}$  are observed and thus fixed. This is indicated by the “;” notation in  $\iota(\mathbf{x}_k; \mathbf{z}_k^{(j)})$ .

Next, the messages  $\kappa(\mathbf{y}_k^{(j)}; \mathbf{z}_k^{(j)})$ ,  $j \in \{1, \dots, J\}$  passed from “ $f(\mathbf{z}_k^{(j)} | \mathbf{x}_k, \mathbf{y}_k^{(j)}, \eta_k^{(j)})$ ” to BS “ $\mathbf{y}_k^{(j)}$ ” are given by

$$\kappa(\mathbf{y}_k^{(j)}; \mathbf{z}_k^{(j)}) = \iint f(\mathbf{z}_k^{(j)} | \mathbf{x}_k, \gamma_k^{(j)}, r_k^{(j)}, \eta_k^{(j)}) \times \alpha(\mathbf{x}_k) \xi(\eta_k^{(j)}) d\mathbf{x}_k d\eta_k^{(j)}. \quad (25)$$

Finally, the messages  $\nu(\eta_k^{(j)}; \mathbf{z}_k^{(j)})$ ,  $j \in \{1, \dots, J\}$  sent from “ $f(\mathbf{z}_k^{(j)} | \mathbf{x}_k, \mathbf{y}_k^{(j)}, \eta_k^{(j)})$ ” to the noise variance nodes “ $\eta_k^{(j)}$ ” are calculated as

$$\nu(\eta_k^{(j)}; \mathbf{z}_k^{(j)}) = \sum_{r_k^{(j)} \in \{0,1\}} \iint f(\mathbf{z}_k^{(j)} | \mathbf{x}_k, \gamma_k^{(j)}, r_k^{(j)}, \eta_k^{(j)}) \times \beta(\gamma_k^{(j)}, r_k^{(j)}) \alpha(\mathbf{x}_k) d\gamma_k^{(j)} d\mathbf{x}_k. \quad (26)$$

These messages provide updated information about the noise variance associated with  $\mathbf{z}_k^{(j)}$ , while taking into account the knowledge of all LOSs states as well as the MT state.

With the BP messages, the beliefs of MT state  $\mathbf{x}_k$ , LOS states  $\mathbf{y}_{k,n}^{(j)}$ ,  $n \in \{1, \dots, N_k^{(j)}\}$ ,  $j \in \{1, \dots, J\}$  and noise variance  $\eta_k^{(j)}$ ,  $j \in \{1, \dots, J\}$  can be obtained as the product of all messages sent to the corresponding variable node, i.e.,

$$\tilde{f}(\mathbf{x}_k) \propto \alpha(\mathbf{x}_k) \prod_{j=1}^J \iota(\mathbf{x}_k; \mathbf{z}_k^{(j)}) \quad (27)$$

$$\tilde{f}(\mathbf{y}_{k,n}^{(j)}) \propto \beta(\mathbf{y}_{k,n}^{(j)}) \kappa(\mathbf{y}_{k,n}^{(j)}; \mathbf{z}_k^{(j)}) \quad (28)$$

$$\tilde{f}(\eta_k^{(j)}) \propto \xi(\eta_k^{(j)}) \nu(\eta_k^{(j)}; \mathbf{z}_k^{(j)}). \quad (29)$$

Computation of these beliefs involves proper normalization such that they integrate and sum to one. The calculated beliefs can then be used for declaration and state estimation as discussed in Section II-C.

#### IV. PARTICLE-BASED IMPLEMENTATION

In general, it is not possible to calculate the beliefs and BP messages discussed in Section III in closed form. This is because the integrations in BP message passing equations (19)–(23) and (24)–(26) as well as message multiplication in belief calculations in (27)–(29) cannot be performed analytically.

Hence, in this section, we present a computationally feasible particle-based implementation [6], [8], [31] of the proposed BP method. The beliefs  $\tilde{f}(\mathbf{x}_k)$ ,  $\tilde{f}(\mathbf{y}_k^{(j)}) = \tilde{f}(\gamma_k^{(j)}, r_k^{(j)})$ , and  $\tilde{f}(\eta_k^{(j)})$  are represented by weighted particle sets  $\{(\mathbf{x}_k^{(p)}, w_{\mathbf{x},k}^{(p)})\}_{p=1}^P$ ,  $\{(\gamma_k^{(j,p)}, w_{\mathbf{y},k}^{(j,p)})\}_{p=1}^P$ , and  $\{(\eta_k^{(j,p)}, w_{\eta,k}^{(j,p)})\}_{p=1}^P$ , for  $j \in \{1, \dots, J\}$ . To obtain linear complexity in  $P$ , we adopt the stacking approach of [32], where particles of the incoming BP messages for each MT–LOS–noise variance tuple are “stacked” into a joint state, requiring the same number of particles  $P$  for all states; this approach is asymptotically optimal. Note that the LOS weights  $w_{\mathbf{y},k}^{(j,p)}$  are not normalized, and their sum  $p_k^{(j)} = \sum_{p=1}^P w_{\mathbf{y},k}^{(j,p)} \approx \int \tilde{f}(\gamma_k^{(j)}, 1) d\gamma_k^{(j)}$  approximates the posterior visibility probability  $f(r_k^{(j)} = 1 \mid \mathbf{z}_{1:k})$ .

The particle-based algorithm at each time step  $k$  consists of a prediction/birth stage followed by a measurement update and belief calculation:

- 1) Prediction and birth: Given  $\{(\mathbf{x}_{k-1}^{(p)}, w_{\mathbf{x},k-1}^{(p)})\}_{p=1}^P$ ,  $\{(\gamma_{k-1}^{(j,p)}, w_{\mathbf{y},k-1}^{(j,p)})\}_{p=1}^P$ , and  $\{(\eta_{k-1}^{(j,p)}, w_{\eta,k-1}^{(j,p)})\}_{p=1}^P$ , the MT state particles  $\mathbf{x}_k^{(p)}$  and noise-variance particles  $\eta_k^{(j,p)}$  are drawn from their transition models with inherited weights, while for each BS  $j$  only  $P' = P - P_a$  propagated LOS particles  $\gamma_k^{(j,p)}$  are retained from the previous step and the remaining  $P_a$  particles are replaced by birth samples from the appearance density, with weights scaled by the visibility probability  $p_v$  and appearance probability  $p_a$ .
- 2) Measurement update and belief calculation: For each stacked particle triplet  $(\mathbf{x}_k^{(p)}, \gamma_k^{(j,p)}, \eta_k^{(j,p)})$ , the covariance  $\mathbf{C}_{\boldsymbol{\theta},k}^{(j)}(\mathbf{p}_k, \gamma_k^{(j,p)}, \eta_k^{(j,p)})$  and corresponding likelihood terms are evaluated, unnormalized importance weights for the BP messages are computed, and normalized to obtain the updated particle beliefs  $\tilde{f}(\mathbf{x}_k)$ ,  $\tilde{f}(\gamma_k^{(j)}, r_k^{(j)})$ , and  $\tilde{f}(\eta_k^{(j)})$  with resampling to prevent particle degeneracy.

An approximation of the MMSE estimates in (14)–(16) at time  $k$  for the MT, LOS, and variance states is obtained directly from the updated weighted particle sets and is given by

$$\hat{\mathbf{x}}_k = \sum_{p=1}^P w_{\mathbf{x},k}^{(p)} \mathbf{x}_k^{(p)} \quad (30)$$

$$\hat{\gamma}_k^{(j)} = \frac{1}{p_k^{(j)}} \sum_{p=1}^P w_{\mathbf{y},k}^{(j,p)} \gamma_k^{(j,p)} \quad (31)$$

$$\hat{\eta}_k^{(j)} = \sum_{p=1}^P w_{\eta,k}^{(j,p)} \eta_k^{(j,p)}. \quad (32)$$

##### A. Efficient Calculation of Likelihood Function

Since the covariance matrix in (9) must be inverted and its determinant evaluated, both of complexity  $\mathcal{O}(M^3)$ , for each particle at each BS when computing the likelihood function in (8), a reduction of the computational complexity is essential.

For a given BS  $j$  and a particle realization of the MT position  $\mathbf{p}_k$ , the covariance matrix in (9) can be expressed as a low-rank perturbation of a scaled identity matrix. Specifically, we collect the LOS and NE components into the matrix

$$\mathbf{U}_k^{(j)} \triangleq [r_k^{(j)} \sqrt{\gamma_k^{(j)}} \mathbf{h}_{\boldsymbol{\chi}}^{\text{lo}(j)}(\mathbf{p}_k) \sqrt{\lambda_{k,\boldsymbol{\theta},1}^{\text{ai}(j)}(\mathbf{p}_k)} \mathbf{h}_{\boldsymbol{\theta},1}^{\text{ai}(j)}(\mathbf{p}_k) \cdots \sqrt{\lambda_{k,\boldsymbol{\theta},D}^{\text{ai}(j)}(\mathbf{p}_k)} \mathbf{h}_{\boldsymbol{\theta},D}^{\text{ai}(j)}(\mathbf{p}_k)] \in \mathbb{C}^{M \times R} \quad (33)$$

where  $R = D + r_k^{(j)} \leq D + 1$ . Using (33), the covariance matrix in (9) can be rewritten as

$$\mathbf{C}_{\boldsymbol{\theta},k}^{(j)} = \eta_k^{(j)} \mathbf{I}_M + \mathbf{U}_k^{(j)} \mathbf{U}_k^{(j)\text{H}}. \quad (34)$$

Applying the Woodbury matrix inversion lemma [33, eq. (159)] and the matrix determinant lemma [34, eq. (B.1.16)], respectively, yields

$$(\mathbf{C}_{\boldsymbol{\theta},k}^{(j)})^{-1} = (\eta_k^{(j)})^{-1} \mathbf{I}_M - (\eta_k^{(j)})^{-2} \mathbf{U}_k^{(j)} \mathbf{G}_k^{(j)-1} \mathbf{U}_k^{(j)\text{H}} \quad (35)$$

where  $\mathbf{G}_k^{(j)} \triangleq \mathbf{I}_R + (\eta_k^{(j)})^{-1} \mathbf{U}_k^{(j)\text{H}} \mathbf{U}_k^{(j)}$  and

$$\log \det(\mathbf{C}_{\boldsymbol{\theta},k}^{(j)}) = M \log(\eta_k^{(j)}) + \log \det(\mathbf{G}_k^{(j)}). \quad (36)$$

Using (35), the quadratic form within the complex Gaussian likelihood function in (8) simplifies to

$$\mathbf{z}_k^{(j)\text{H}} (\mathbf{C}_{\boldsymbol{\theta},k}^{(j)})^{-1} \mathbf{z}_k^{(j)} = \|\mathbf{q}_k^{(j)}\|^2 - \|\mathbf{G}_k^{(j)-1/2} \mathbf{B}_k^{(j)\text{H}} \mathbf{q}_k^{(j)}\|^2. \quad (37)$$

where  $\mathbf{q}_k^{(j)} \triangleq (\eta_k^{(j)})^{-1/2} \mathbf{z}_k^{(j)}$  and  $\mathbf{B}_k^{(j)} \triangleq (\eta_k^{(j)})^{-1/2} \mathbf{U}_k^{(j)}$ . Substituting (37) and (36) into (8), the log-likelihood function in (8) can be rewritten as

$$\begin{aligned} \log f_{\boldsymbol{\theta}}(\mathbf{z}_k^{(j)} \mid \mathbf{x}_k, \mathbf{y}_k^{(j)}, \eta_k^{(j)}) \\ = -\|\mathbf{q}_k^{(j)}\|^2 + \|\mathbf{G}_k^{(j)-1/2} \mathbf{B}_k^{(j)\text{H}} \mathbf{q}_k^{(j)}\|^2 \\ - \log \det(\mathbf{G}_k^{(j)}) - M \log(\pi \eta_k^{(j)}) \end{aligned} \quad (38)$$

which requires only inversion and determinant computation of the  $R \times R$  matrix  $\mathbf{G}_k^{(j)}$ , with  $R = D + r_k^{(j)} \ll M$ . Hence, the computational complexity per likelihood evaluation is reduced from  $\mathcal{O}(M^3)$  to  $\mathcal{O}(MR^2 + R^3)$ . Notably,  $JP$  computations across BSs and particles can be computed in parallel.

*Remark:* Since the LOS contribution is rank-one, the two cases  $r_k^{(j)} \in \{0, 1\}$  differ only by the presence of a single column in (33). This structure enables efficient rank-one updates when calculating the likelihood function in (8) for  $r_k^{(j)} = 0$  and  $r_k^{(j)} = 1$ , respectively.

#### V. VARIATIONAL UNSUPERVISED LEARNING

We assume that the MT states  $\mathbf{x}_{0:k}$ , the LOS states  $\mathbf{y}_{0:k} = [\mathbf{r}_{0:k} \ \boldsymbol{\gamma}_{0:k}]^T$ , and noise variances  $\boldsymbol{\eta}_{0:k}$  are latent variables for all BS  $j \in \{1, 2, \dots, J\}$  and time steps  $\{0, 2, \dots, k\}$ . The proposed unsupervised learning algorithm learns the AI parametrization  $\boldsymbol{\theta}$  by maximizing the marginal likelihood function, i.e., *evidence*, given all measurements  $\mathbf{z}_{1:k}$ , i.e.,

$$\begin{aligned} \boldsymbol{\theta}^* &= \arg \max_{\boldsymbol{\theta}} \log f_{\boldsymbol{\theta}}(\mathbf{z}_{1:k}) \\ &= \arg \max_{\boldsymbol{\theta}} \log \sum_{\mathbf{r}_{0:k}} \cdots \sum_{\mathbf{x}_{0:k} \boldsymbol{\gamma}_{0:k} \boldsymbol{\eta}_{0:k}} \int \cdots \int \\ &\quad \times f_{\boldsymbol{\theta}}(\mathbf{x}_{0:k}, \mathbf{r}_{0:k}, \boldsymbol{\gamma}_{0:k}, \boldsymbol{\eta}_{0:k}, \mathbf{z}_{1:k}) d\mathbf{x}_{0:k} d\boldsymbol{\gamma}_{0:k} d\boldsymbol{\eta}_{0:k}. \end{aligned} \quad (39)$$

Since direct maximization of (39) is intractable due to the high-dimensional integrals and features and the summation over the discrete LOS variables, we resort to an variational-based learning framework. Following [19], for any auxiliary

density  $q(\mathbf{x}_{0:k}, \mathbf{y}_{0:k}, \boldsymbol{\eta}_{0:k})$ , we can decompose the marginal log-likelihood function as

$$\log f_{\tilde{\boldsymbol{\theta}}}(\mathbf{z}_{1:k}) = \mathcal{L}(q(\mathbf{x}_{0:k}, \mathbf{y}_{0:k}, \boldsymbol{\eta}_{0:k}; \tilde{\boldsymbol{\theta}}) + \text{KL}(q(\mathbf{x}_{0:k}, \mathbf{y}_{0:k}, \boldsymbol{\eta}_{0:k}), f_{\tilde{\boldsymbol{\theta}}}(\mathbf{x}_{0:k}, \mathbf{y}_{0:k}, \boldsymbol{\eta}_{0:k} | \mathbf{z}_{1:k})) \quad (40)$$

where  $\text{KL}(\cdot, \cdot)$  is the Kullback–Leibler divergence (KLD) and

$$\begin{aligned} & \mathcal{L}(q(\mathbf{x}_{0:K}, \mathbf{r}_{0:k}, \boldsymbol{\gamma}_{0:k}, \boldsymbol{\eta}_{0:k}; \tilde{\boldsymbol{\theta}})) \\ &= \sum_{\mathbf{r}_{0:k}} \cdots \sum_{\mathbf{x}_{0:k}} \int \cdots \int_{\boldsymbol{\gamma}_{0:k} \boldsymbol{\eta}_{0:k}} q(\mathbf{x}_{1:K}, \mathbf{r}_{0:k}, \boldsymbol{\gamma}_{0:k}, \boldsymbol{\eta}_{0:k}) \\ & \times \log \frac{f_{\tilde{\boldsymbol{\theta}}}(\mathbf{x}_{0:k}, \mathbf{r}_{0:k}, \boldsymbol{\gamma}_{0:k}, \boldsymbol{\eta}_{0:k} | \mathbf{z}_{1:k})}{q(\mathbf{x}_{0:K}, \mathbf{r}_{0:k}, \boldsymbol{\gamma}_{0:k}, \boldsymbol{\eta}_{0:k})} d\mathbf{x}_{1:k} d\boldsymbol{\gamma}_{0:k} d\boldsymbol{\eta}_{0:k}. \quad (41) \end{aligned}$$

represents the ELBO. Since the KLD is non-negative, the ELBO  $\mathcal{L}(q(\mathbf{x}_{0:K}, \mathbf{r}_{0:k}, \boldsymbol{\gamma}_{0:k}, \boldsymbol{\eta}_{0:k}; \tilde{\boldsymbol{\theta}}))$  is a lower bound on the marginal log-likelihood function with equality, if and only if,  $q(\mathbf{x}_{0:K}, \mathbf{r}_{0:k}, \boldsymbol{\gamma}_{0:k}, \boldsymbol{\eta}_{0:k}) = f_{\tilde{\boldsymbol{\theta}}}(\mathbf{x}_{0:k}, \mathbf{r}_{0:k}, \boldsymbol{\gamma}_{0:k}, \boldsymbol{\eta}_{0:k} | \mathbf{z}_{1:k})$  [19], [35].

Based on this rationale, we formulate a two step iterative algorithm that maximizes the ELBO using the cost function  $q^{(t)}(\mathbf{x}_{0:k}, \mathbf{y}_{0:k}, \boldsymbol{\eta}_{0:k}) = f_{\tilde{\boldsymbol{\theta}}_t}(\mathbf{x}_{0:k}, \mathbf{y}_{0:k}, \boldsymbol{\eta}_{0:k} | \mathbf{z}_{1:k})$ , with  $\tilde{\boldsymbol{\theta}}_t$  being the current AI parametrization, yielding the auxiliary function

$$\begin{aligned} Q(\tilde{\boldsymbol{\theta}} | \tilde{\boldsymbol{\theta}}_t) & \triangleq \mathbb{E}_{f_{\tilde{\boldsymbol{\theta}}_t}(\mathbf{x}_{0:k}, \mathbf{y}_{0:k}, \boldsymbol{\eta}_{0:k} | \mathbf{z}_{1:k})} [\log f_{\tilde{\boldsymbol{\theta}}}(\mathbf{x}_{0:k}, \mathbf{y}_{0:k}, \boldsymbol{\eta}_{0:k}, \mathbf{z}_{1:k})] \\ &= \sum_{k'=1}^k \sum_{j=1}^J \mathbb{E}_{f_{\tilde{\boldsymbol{\theta}}_t}(\mathbf{x}_{k'}, \mathbf{y}_{k'}, \boldsymbol{\eta}^{(j)} | \mathbf{z}_{k'})} [\log f_{\tilde{\boldsymbol{\theta}}}(\mathbf{z}_{k'}^{(j)} | \mathbf{x}_{k'}, \mathbf{y}_{k'}, \boldsymbol{\eta}_{k'}^{(j)})] \quad (42) \end{aligned}$$

where we have exploited the factorization of the posterior PDF in (18).

1) *Inference Step (SPA Algorithm)*: The posterior PDF  $q^{(t)}(\mathbf{x}_{0:k}, \mathbf{y}_{0:k}, \boldsymbol{\eta}_{0:k}) = f_{\tilde{\boldsymbol{\theta}}_t}(\mathbf{x}_{0:k}, \mathbf{y}_{0:k}, \boldsymbol{\eta}_{0:k} | \mathbf{z}_{1:k})$  required in (42) is approximated using the SPA algorithm of Section IV. Since we perform resampling after each measurement update, we only need the particles of the MT state and the variances for each BS  $\mathbf{x}_{k'}^{(p)}$  and  $\boldsymbol{\eta}_{k'}^{(j,p)}$  as well as the particles and existence probabilities of the LOS states  $\gamma_{k'}^{(j,p)}$  and  $p_{k'}^{(j)}$  to approximate  $Q(\tilde{\boldsymbol{\theta}} | \tilde{\boldsymbol{\theta}}_t)$  in (42), i.e.,

$$\begin{aligned} \tilde{Q}(\tilde{\boldsymbol{\theta}} | \tilde{\boldsymbol{\theta}}_t) &= \sum_{k'=1}^k \sum_{j=1}^J \frac{1}{P} \sum_{p=1}^P \left( p_{k'}^{(j)} \log \mathcal{CN}(\mathbf{z}_{k'}^{(j)}; \mathbf{0}, \mathbf{C}_{\tilde{\boldsymbol{\theta}}, n, 1}^{(j,p)}) \right. \\ & \left. + (1 - p_{k'}^{(j)}) \log \mathcal{CN}(\mathbf{z}_{k'}^{(j)}; \mathbf{0}, \mathbf{C}_{\tilde{\boldsymbol{\theta}}, n, 0}^{(j,p)}) \right) \quad (43) \end{aligned}$$

$$= \sum_{k'=1}^k \tilde{Q}_k(\tilde{\boldsymbol{\theta}} | \tilde{\boldsymbol{\theta}}_t) \quad (44)$$

with  $\mathbf{C}_{\tilde{\boldsymbol{\theta}}, n, 1}^{(j,p)} \triangleq \mathbf{C}_{\tilde{\boldsymbol{\theta}}, k}^{(j)}(\mathbf{p}_k^{(p)}, \gamma_k^{(j,p)}, 1, \boldsymbol{\eta}_k^{(j,p)})$  and  $\mathbf{C}_{\tilde{\boldsymbol{\theta}}, n, 0}^{(j,p)} \triangleq \mathbf{C}_{\tilde{\boldsymbol{\theta}}, k}^{(j)}(\mathbf{p}_k^{(p)}, \gamma_k^{(j,p)}, 0, \boldsymbol{\eta}_k^{(j,p)})$ .

2) *Learning Step (Unsupervised AI Model Learning)*: The updated parametrization  $\tilde{\boldsymbol{\theta}}_{t+1}$  is determined by maximizing (43), i.e.,

$$\tilde{\boldsymbol{\theta}}_{t+1} = \arg \max_{\tilde{\boldsymbol{\theta}}} \tilde{Q}(\tilde{\boldsymbol{\theta}} | \tilde{\boldsymbol{\theta}}_t). \quad (45)$$

## VI. DATA-DRIVEN MODELS

The data-driven components introduced in the measurement model in Section II-A parameterize environment-induced multipath contributions via the mappings in (6) and (7). These

mappings are implemented using deep neural networks (DNNs) and jointly define a position-dependent generative model of the RF propagation environment. The concept is shown in Fig 1.

a) *NN Inputs*: For each BS  $j$ , the NNs are conditioned solely on the BS position  $\mathbf{p}^{(j)} \in \mathbb{R}^d$ , which serve as the input to the model. This parametrization allows the network to capture site-specific propagation characteristics and environment-dependent effects associated with each BS location, while remaining independent of the instantaneous MT position. If required,  $\mathbf{p}^{(j)}$  can be augmented with positional encodings to better represent fine-grained spatial variations, yielding an effective input dimension of  $D_{\text{in}} = d + N_{\text{enc}}d$ .

b) *NN Architecture and Outputs*: Given the input  $\mathbf{p}^{(j)}$ , the NNs predict the parameters of the environment-induced multipath model via the mappings  $f_{\mathbf{p}, \boldsymbol{\theta}}^{\text{ai}}(\mathbf{p}^{(j)}) \in \mathbb{R}^{d+1 \times D}$  in (6) and  $f_{\rho, \boldsymbol{\theta}}^{\text{ai}}(\mathbf{p}^{(j)}) \in \mathbb{R}^{1 \times D}$  in (7). These outputs define the predicted map features  $\mathbf{P}_{\boldsymbol{\theta}}^{\text{ai}(j)}$ , from which the corresponding delays, DoAs, and power-related variances  $\boldsymbol{\lambda}_{\boldsymbol{\theta}}^{\text{ai}(j)}$  of the  $D$  environment-induced MPCs are obtained and used to directly parameterize the covariance matrix in (9). Specifically,  $f_{\mathbf{p}, \boldsymbol{\theta}}^{\text{ai}}(\mathbf{p}^{(j)})$  is implemented by a three-layered multi-layer perceptron (MLP) with ReLU activation functions and hidden-layer dimensions  $\{L_{\mathbf{p}, 1}, L_{\mathbf{p}, 2}, d \times 3D\}$ . To guarantee strictly positive biases,  $b_{\boldsymbol{\theta}, n}^{\text{ai}(j)}$  is constrained via the absolute-value mapping  $|\cdot|$ . Likewise,  $f_{\rho, \boldsymbol{\theta}}^{\text{ai}}(\mathbf{p}^{(j)})$  is implemented as a three-layer MLP with hidden dimensions  $\{L_{\rho, 1}, L_{\rho, 2}\}$  and output size  $D$ . Strictly positive real-valued variances are enforced by applying the absolute value  $|\cdot|$  to the outputs of  $f_{\rho, \boldsymbol{\theta}}^{\text{ai}}(\mathbf{p}^{(j)})$ .

c) *Learning Schemes*: All NN parameters  $\boldsymbol{\theta}$  and unknown array response parameters  $\boldsymbol{\chi}$  are learned in an unsupervised manner using the cost function in (45). The NN parameters are updated to  $\boldsymbol{\theta}_{t+1}$  while keeping  $\boldsymbol{\chi} = \boldsymbol{\chi}_t$  fixed, with  $\boldsymbol{\theta}_t$  and  $\boldsymbol{\chi}_t$  used to evaluate the cost function. Conversely, the array response parameters are updated to  $\boldsymbol{\chi}_{t+1}$  while keeping  $\boldsymbol{\theta} = \boldsymbol{\theta}_t$  fixed, again using the same cost function.

1) *MT Track Segmentation and Online Learning*: Learning can be performed using the full track  $\mathbf{z}_{1:K}$  ( $K$  is the last time step of a track) or shorter track segments  $\mathbf{z}_{k-k_0:k}$ . Accordingly, the parameters  $\tilde{\boldsymbol{\theta}}$  are obtained by maximizing the accumulated objective in (44) by summing  $\tilde{Q}_k(\tilde{\boldsymbol{\theta}} | \tilde{\boldsymbol{\theta}}_t)$  over the corresponding time indices and using an Adam-optimizer to learn the parametrizations of the NNs.

2) *Approximate Representations*: To reduce the computational complexity of the learning step, we employ two approximation schemes: (1) only a subset of  $P_0 < P$  particles is retained after resampling, and (2) the particle-based beliefs of the MT state  $\mathbf{x}_k^{(p)}$  and the latent variables  $\gamma_k^{(j,p)}$  and  $\boldsymbol{\eta}_k^{(j,p)}$  are replaced by their MMSE estimates given in (30), (31), and (32), respectively. Furthermore, if ground-truth MT positions  $\mathbf{x}_k^{\text{gt}}$  are available, partially supervised learning can be performed by conditioning the cost function on  $\mathbf{x}_k^{\text{gt}}$  instead of  $\hat{\mathbf{x}}_{k, \text{MMSE}}$ .

3) *Learning of Response Parameters  $\boldsymbol{\chi}$  (optional)*: Since  $\boldsymbol{\chi}$  enters the likelihood function in (8) through the response vector  $\mathbf{h}_{\boldsymbol{\chi}}(\cdot)$ , the gradient of the cost function in (44) with respect to  $\boldsymbol{\chi}$  is used to learn these parameters via Adam-optimizer, while keeping  $\boldsymbol{\theta} = \boldsymbol{\theta}_t$  fixed. This enables data-driven calibration of the response vector  $\mathbf{h}_{\boldsymbol{\chi}}(\cdot)$  in (2) directly from raw measurements.

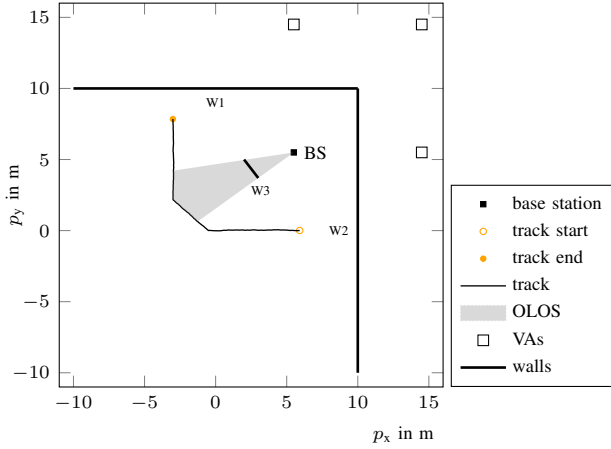


Fig. 2. Graphical representation of the investigated synthetic experiment: Fig. (a) shows the simulated trajectory, the (single) known BS position, unknown walls (and respective virtual anchors (VAs) and indices the OLOS situation.

## VII. RESULTS

We compare (i) the proposed AI-enhanced direct SLAM method with (ii) a direct LOS-only SPA (the AI-induced covariance term in (9) is deactivated) and (iii) a genie-aided direct SPA (true map features are used in covariance matrix in (9), cf. [36]). The simple multipath propagation environment and chosen AI model are used solely to demonstrate that the unsupervised approach can learn the generative signal model (map features and amplitude statistics) in a controlled scenario; the framework and AI components can be flexibly scaled without altering the learning principle.

1) *Simulation Setup and Scenario*: We evaluate the proposed algorithm using synthetic radio measurements that were generated using the measurement model in (1). We use the simple scenario presented in Fig. 2, where the MT receives radio signals from only a single BS, while moving along an unsteady track with two distinct direction changes. It is observed at 190 discrete time steps  $k$  at a constant observation rate of 100 ms. The ground truth MPC distances are calculated based on the simple floor plan of Fig. 2 (W1 and W2) using the image source or VA model [7], [37] considering single bounce and double bounce reflections. The amplitudes of the LOS component as well as the MPCs are assumed to follow free-space path loss according to their individual propagation paths, and determined by a SNR of 42 dB at a distance of 1 m. The amplitudes of MPCs are additionally attenuated by 3 dB per reflection. The BS is obstructed by an obstacle (W3), which leads to an OLOS situation in the center of the track. We choose the transmitted signal to be of root-raised-cosine shape with a roll-off factor of 0.6 and a 3-dB bandwidth of 500 MHz at a center frequency of  $f_c = 7$  GHz. The received baseband signal is critically sampled, i.e.,  $T_s = 1.25$  ns, with a total number of  $N_s = 81$  samples, amounting to a maximum distance  $d_{\max} = 30$  m. We use a uniform rectangular array with  $M_a = 4$  spaced at  $\lambda/2$  with  $\lambda = c/f_c$ . The state transition PDF  $f(\mathbf{x}_n|\mathbf{x}_{n-1})$  of the MT state  $\mathbf{x}_n$  is described by a linear, constant-velocity and stochastic-acceleration model [38, p. 273], given as  $\mathbf{x}_n = \mathbf{A} \mathbf{x}_{n-1} + \mathbf{B} \mathbf{w}_n$  with the acceleration process  $\mathbf{w}_n$  being i.i.d. across  $n$ , zero mean, and Gaussian with covariance matrix  $\sigma_a^2 \mathbf{I}_2$ , the acceleration standard deviation  $\sigma_a$ , and  $\mathbf{A} \in \mathbb{R}^{4 \times 4}$  and  $\mathbf{B} \in \mathbb{R}^{4 \times 2}$  being defined according to [38, p. 273]. The acceleration standard deviation is set to

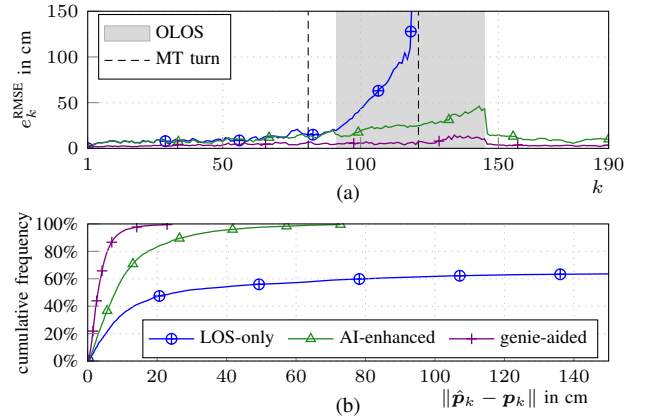


Fig. 3. Performance in terms of the RMSE of the estimated MT position over time  $n$  (a) and as the cumulative frequency of the magnitude error of the estimated MT position (b). The gray area represents the area of OLOS between BS and MT according to Fig. 2.

$\sigma_a = 2$  m/s<sup>2</sup> assuming that it is estimated by an IMU sensor. The particles for the initial MT position and velocity at  $k = 0$  are drawn i.i.d. from Gaussian distributions, whose mean for each realization is itself sampled from a Gaussian centered at the true MT state, with initialization standard deviations of 0.5 m and 0.1 m/s. The state-transition parameters for the amplitude and noise states are set to  $c_\gamma = 100$  and  $c_\eta = 100$ . The numbers of particles are  $P = 5000$  and  $P_a = 250$ , respectively. The appearance and visibility probabilities are  $p_a = 0.01$  and  $p_v = 0.95$ , and the appearance prior  $f_a(\gamma_k^{(j)})$  is uniform on  $[0, 2]$ . The initial distributions for noise variance  $f(\eta_0^{(j)})$  and LOS amplitude variance  $f(\gamma_0^{(j)})$  for each BS are uniformly distributed on  $[0, 5 \cdot 10^{-4}]$  and  $[0, 2]$ , respectively. The initial LOS existences probability is  $f(r_0^{(j)}) = 0.5$  for each BS.

For implementation, we use Python with PyTorch and the Adam optimizer with default parameters ( $\beta_1 = 0.9$ ,  $\beta_2 = 0.999$ ,  $\epsilon = 10^{-8}$ ). Separate learning rates are used for the two networks, i.e.,  $10^{-4}$  for the amplitude NN and  $5 \cdot 10^{-3}$  for the map-feature NN. Unsupervised updates are performed every  $k_0 = 30$  time steps (track segment) using  $P_0 = 30$  particles drawn from the respective marginal posterior PDFs, with 300 backpropagation iterations per segment. The number of AI components  $D = 30$ . To prevent an initially concentrated map and encourage exploration during early online updates, the neural map features  $\mathbf{p}_{\theta,n}^{\text{ai}(j)}$  are initialized such that their decoded means are uniformly distributed over a predefined region  $([-35 \text{ m}, 35 \text{ m}] \times [-35 \text{ m}, 35 \text{ m}])$ .<sup>4</sup>

2) *Numerical Experiment*: Fig. 3 presents the numerical results in terms of the RMSE of the estimated MT position over time,  $e_k^{\text{RMSE}} = \mathbb{E}_{\mathbf{p}_k}[\|\hat{\mathbf{p}}_k - \mathbf{p}_k\|^2]^{1/2}$ , and the cumulative distribution of the position error magnitude, averaged over 50 simulation runs. Without any prior floorplan information, the proposed method learns the feature map and amplitude statistics from the geometric information obtained in the initial phase of the track. Hence, it can maintain accurate localization in the OLOS situation despite the single BS setup, with the error staying below 75 cm in all realizations, where the direct LOS-only algorithm diverges. Its performance approaches that

<sup>4</sup>The final linear layer is calibrated by evaluating the BS inputs  $\mathbf{p}^{(j)}$  and solving a least-squares fit from the last hidden features to uniformly sampled features  $\mathbf{P}_\theta^{\text{ai}(j)}$  in (6), yielding map features that span the area of interest while preserving the network architecture.

of the genie-aided direct SPA, which serves as a lower bound in the considered scenario. Since the proposed particle-based implementation can be executed in parallel over particles  $P$  and anchors  $J$ , we used a GPU-based implementation. The mean runtime of the AI-enhanced algorithm was 30 ms per time  $k$  (even for  $D = 30$ ) for the *inference step* and 250 ms for the *unsupervised track-segment learning step*.

### VIII. CONCLUSION

We presented an AI-enhanced direct SLAM method that combines Bayesian inference on raw RF signals with unsupervised environment learning. The proposed method combines model-based components (capturing the LOS contribution) with learned AI components (capturing the environment-induced MPCs) in order to retain a physically consistent signal model that explicitly models the sampled RF signal spectrum and array response and that learns the environment in terms of MPC statistics and propagation geometry. The proposed ELBO maximization enables principled unsupervised training of the generative environment model without requiring labeled positions or map features. Numerical results in a simple multipath scenario demonstrate that the learned model effectively captures environment geometry and amplitude statistics and, thus, supports accurate MT localization, especially under OLOS conditions. Potential directions for future research include introducing partially modeled map features and hierarchical feature models [8], [39], incorporating uncertainty-aware environment representations, and validating performance on real-world measurement data to further improve generalization and practical deployment.

### REFERENCES

- [1] N. González-Prelcic *et al.*, “The integrated sensing and communication revolution for 6G: Vision, techniques, and applications,” *Proc. IEEE*, vol. 112, pp. 676–723, May 2024.
- [2] K. Witrisal *et al.*, “High-accuracy localization for assisted living: 5G systems will turn multipath channels from foe to friend,” *IEEE Signal Process. Mag.*, vol. 33, pp. 59–70, Mar. 2016.
- [3] C. Gentner, T. Jost, W. Wang, S. Zhang, A. Dammann, and U.-C. Fiebig, “Multipath assisted positioning with simultaneous localization and mapping,” *IEEE Trans. Wireless Commun.*, vol. 15, pp. 6104–6117, June 2016.
- [4] T. L. Hansen, B. H. Fleury, and B. D. Rao, “Superfast line spectral estimation,” *IEEE Trans. Signal Process.*, vol. PP, pp. 1–1, Feb. 2018.
- [5] S. Grebien, E. Leitinger, K. Witrisal, and B. H. Fleury, “Super-resolution estimation of UWB channels including the dense component – An SBL-inspired approach,” *IEEE Trans. Wireless Commun.*, vol. 23, pp. 10301–10318, Feb. 2024.
- [6] E. Leitinger, F. Meyer, F. Hlawatsch, K. Witrisal, F. Tufvesson, and M. Z. Win, “A belief propagation algorithm for multipath-based SLAM,” *IEEE Trans. Wireless Commun.*, vol. 18, pp. 5613–5629, Dec. 2019.
- [7] E. Leitinger, A. Venus, B. Teague, and F. Meyer, “Data fusion for multipath-based SLAM: Combining information from multiple propagation paths,” *IEEE Trans. Signal Process.*, vol. 71, pp. 4011–4028, Sep. 2023.
- [8] M. Liang, E. Leitinger, and F. Meyer, “Direct multipath-based SLAM,” *IEEE Trans. Signal Process.*, vol. 73, pp. 2336–2352, Mar. 2025.
- [9] H. Kim, K. Granstrom, L. Svensson, S. Kim, and H. Wymeersch, “PMBM-based SLAM filters in 5G mmWave vehicular networks,” *IEEE Trans. Veh. Technol.*, pp. 1–1, May 2022.
- [10] Y. Ge, O. Kaltiokallio, Y. Xia, A. F. Garcia-Fernandez, H. Kim, J. Talvitie, M. Valkama, H. Wymeersch, and L. Svensson, “Batch SLAM with PMBM data association sampling and graph-based optimization,” *IEEE Trans. Signal Process.*, vol. 73, pp. 2139–2153, May 2025.
- [11] A. Salihu, M. Rupp, and S. Schwarz, “Self-supervised and invariant representations for wireless localization,” *IEEE Trans. Wireless Commun.*, vol. 23, no. 8, pp. 8281–8296, 2024.
- [12] G. Pan, K. Huang, H. Chen, S. Zhang, C. Häger, and H. Wymeersch, “Large wireless localization model (LWLM): A foundation model for positioning in 6g networks,” *ArXiv e-prints*, 2025.
- [13] N. Shlezinger, N. Farsad, Y. C. Eldar, and A. J. Goldsmith, “Learned factor graphs for inference from stationary time sequences,” *IEEE Trans. Signal Process.*, vol. 70, pp. 366–380, 2022.
- [14] N. Shlezinger, J. Whang, Y. C. Eldar, and A. G. Dimakis, “Model-based deep learning,” *Proc. IEEE*, vol. 111, pp. 465–499, Mar. 2023.
- [15] A. Venus, E. Leitinger, S. Tertinek, and K. Witrisal, “A neural-enhanced factor graph-based algorithm for robust positioning in obstructed LOS situations,” *IEEE Open J. of Signal Process.*, vol. 5, pp. 29–38, Nov. 2023.
- [16] J. P. Merkofer *et al.*, “DA-MUSIC: Data-driven DoA estimation via deep augmented MUSIC algorithm,” *IEEE Trans. Veh. Technol.*, vol. 73, pp. 2771–2785, Sept. 2024.
- [17] B. Chatelier, V. Corlay, M. Crussière, and L. L. Magoarou, “Model-based learning for multi-antenna multi-frequency location-to-channel mapping,” *arXiv preprint*, 2025.
- [18] S. Wei, M. Liang, and F. Meyer, “Bayesian multiobject tracking with neural-enhanced motion and measurement models,” *IEEE Trans. Signal Process.*, pp. 1–16, Jan. 2026.
- [19] D. G. Tzikas, A. C. Likas, and N. P. Galatsanos, “The variational approximation for Bayesian inference,” *IEEE Signal Process. Mag.*, vol. 25, pp. 131–146, Nov. 2008.
- [20] M. J. Johnson, D. K. Duvenaud, A. Wiltchko, R. P. Adams, and S. R. Datta, “Composing graphical models with neural networks for structured representations and fast inference,” in *Proc. NeurIPS-2016*, (Barcelona, Spain), Dec. 2016.
- [21] K. Greff, S. van Steenkiste, and J. Schmidhuber, “Neural expectation maximization,” in *Proc. NeurIPS-2017*, (Red Hook, NY, USA), pp. 6694–6704, Dec. 2017.
- [22] A. Richter, *Estimation of Radio Channel Parameters: Models and Algorithms*. PhD thesis, Ilmenau University of Technology, 2005.
- [23] A. Fascista, B. J. B. Deutschmann, M. F. Keskin, T. Wilding, A. Coluccia, K. Witrisal, E. Leitinger, G. Seco-Granados, and H. Wymeersch, “Joint localization, synchronization and mapping via phase-coherent distributed arrays,” *IEEE J. Sel. Topics Signal Process.*, pp. 1–16, Jan. 2025.
- [24] D. P. Wipf and B. D. Rao, “An empirical Bayesian strategy for solving the simultaneous sparse approximation problem,” *IEEE Trans. Signal Process.*, vol. 55, pp. 3704–3716, July 2007.
- [25] M.-A. Badiu, T. L. Hansen, and B. H. Fleury, “Variational Bayesian inference of line spectra,” *IEEE Trans. Signal Process.*, vol. 65, pp. 2247–2261, Jan. 2017.
- [26] A. Lepoutre, O. Rabaste, and F. Le Gland, “Multitarget likelihood computation for track-before-detect applications with amplitude fluctuations of type Swerling 0, 1, and 3,” *IEEE Trans. Aerosp. Electron. Syst.*, vol. 52, pp. 1089–1107, June 2016.
- [27] L. E. Leitinger, Wielandner, A. Venus, and K. Witrisal, “Multipath-based SLAM for cooperative navigation and map fusion,” in *Proc. Asilomar-24*, (Pacific Grove, CA, USA), Oct. 2024.
- [28] F. Kschischang, B. Frey, and H.-A. Loeliger, “Factor graphs and the sum-product algorithm,” *IEEE Trans. Inf. Theory*, vol. 47, pp. 498–519, Feb. 2001.
- [29] J. Yedidia, W. Freemand, and Y. Weiss, “Constructing free-energy approximations and generalized belief propagation algorithms,” *IEEE Trans. Inf. Theory*, vol. 51, pp. 2282–2312, July 2005.
- [30] D. Koller and N. Friedman, *Probabilistic Graphical Models: Principles and Techniques*. Cambridge, MA: MIT Press, 2009.
- [31] M. S. Arulampalam, S. Maskell, N. Gordon, and T. Clapp, “A tutorial on particle filters for online nonlinear/non-Gaussian Bayesian tracking,” *IEEE Trans. Signal Process.*, vol. 50, pp. 174–188, Feb. 2002.
- [32] F. Meyer, O. Hlinka, H. Wymeersch, E. Riegler, and F. Hlawatsch, “Distributed localization and tracking of mobile networks including noncooperative objects,” *IEEE Trans. Signal Inf. Process. Netw.*, vol. 2, pp. 57–71, Mar. 2016.
- [33] K. B. Petersen and M. S. Pedersen, *The Matrix Cookbook*. Technical University of Denmark, Nov. 2012. Version 2012-11-15.
- [34] C. Pozrikidis, *An Introduction to Grids, Graphs, and Networks*. Oxford University Press, 2014.
- [35] C. M. Bishop, *Pattern Recognition and Machine Learning (Information Science and Statistics)*. Berlin, Heidelberg: Springer-Verlag, 2006.
- [36] E. Leitinger, F. Meyer, P. Meissner, K. Witrisal, and F. Hlawatsch, “Belief propagation based joint probabilistic data association for multipath-assisted indoor navigation and tracking,” in *Proc. ICL-GNSS-16*, (Barcelona, Spain), pp. 1–6, June 2016.
- [37] T. Pedersen, “Stochastic multipath model for the in-room radio channel based on room electromagnetics,” *IEEE Trans. Antennas Propag.*, vol. 67, pp. 2591–2603, April 2019.
- [38] Y. Bar-Shalom, X. R. Li, and T. Kirubarajan, *Estimation with Applications to Tracking and Navigation: Algorithms and Software for Information Extraction*. Hoboken, NJ: John Wiley and Sons, 2001.
- [39] X. Li, B. J. B. Deutschmann, E. Leitinger, and F. Meyer, “Adaptive multipath-based SLAM for distributed MIMO systems,” *ArXiv e-prints*, 2025.